Synthesis and Characterization of Bis(3,4-ethylene-dioxythiophene)-(4,4′-dialkyl-2,2′-bithiazole) Co-oligomers for Electronic Applications

Jie Cao, Jeff W. Kampf, and M. David Curtis*

Department of Chemistry and the Macromolecular Science and Engineering Center, University of Michigan, Ann Arbor, Michigan 48109-1055

Received July 23, 2002. Revised Manuscript Received November 4, 2002

The synthesis and characterization of several co-oligomers, 5,5′-bis(4,4′-dialkyl-2,2′-bithiazol-5-yl)-(3,4,3′,4′-bis(ethylenedioxy)-2,2′-dithienyl) (AT_2A), 5,5′-bis(3,4-ethylenedioxythien-2-yl)-4,4′-dibutyl-2,2′-bithiazole (TBT), and 5,5′-bis(3,4,3′,4′-bis(ethylenedioxy)-2,2′-dithien-5-yl)-4,4′-dibutyl-2,2′-bithiazole (T_2BT_2) are described. The solid-state structure of AT_2A features π-stacking with a short intermolecular distance of 3.5 Å. In thin films, the π-stacks are parallel to the film substrate as determined by X-ray diffraction. The UV−vis spectra of AT_2A films show features that are ascribed to the effects of π-stacking. In addition, all these co-oligomers, composed of donor−acceptor moieties, show lowered optical band gaps, mainly because of the low oxidation potential imparted by incorporation of the 3,4-ethylenedioxythiophene (EDOT) moiety. Cyclic voltammetry indicates that these co-oligomers can be either p-doped or n-doped, and the spectroelectrochemical measurements show that the AT_2A films are stable upon cycling the oxidation state. All these features make these materials promising for use in electronic devices, e.g., organic thin film transistors.

Introduction

Recently, organic conjugated materials have been studied very intensively as active materials for organic thin film transistors (OTFTs).[1−5] The unique properties of these organic materials make them more attractive than inorganic semiconductors for applications requiring large area coverage, structural flexibility, or solution processing.[6−8] Currently, outstanding progress has been made in fabricating OTFT devices.[9−12] The field-effect mobility of some OTFT devices has reached values comparable to those of amorphous Si-TFTs, e.g., single-crystal pentacene OTFT devices show mobilities of 1−2.7 $cm^2V^{-1}s^{-1}$ at room temperature,[9,13] a value comparable to that of amorphous Si. These advances in organic devices suggest that organic conjugated materials may be competitive with traditional Si technology in low-end applications that do not require rapid switching rates. However, some fundamental challenges still remain, and, above all, there remain questions about how charge transport is related to the molecular and solid-state structures of the organic materials.[14−17] In OTFT devices, early success has been limited to a few types of conjugated materials,[18] e.g., thiophene oligomers, polythiophene, pentacene, etc. It is well-known that both thiophene oligomers and pentacene molecules are packed in the so-called "herringbone" pattern in which intermolecular, $\pi-\pi$ contacts are minimized.[19−21] Despite the poor $\pi-\pi$ overlap between neighboring molecules, highly purified pentacene has extremely high charge carrier mobility at low temperature.[9,10] There is little evidence to indicate that the herringbone-packing pattern is structurally superior for promoting high carrier mobility to other crystalline prototypes, e.g., π-stacks. Therefore, it is important to

* To whom correspondence should be addressed. Phone: 734-763-2132. Fax: 734-763-2307. E-mail: mdcurtis@umich.edu.

(1) Dimitrakopoulos, C. D.; Malenfant, P. R. L. *Adv. Mater.* **2002**, *14*, 99.
(2) Horowitz, G. *Adv. Mater.* **1998**, *10*, 365.
(3) Horowitz, G. *J. Mater. Chem.* **1999**, *9*, 2021.
(4) Katz, H. E.; Bao, Z. *J. Phys. Chem. B* **2000**, *104*, 671.
(5) Lovinger, A. J.; Rothberg, L. J. *J. Mater. Res.* **1996**, *11*, 1581.
(6) Drury, C. J.; Mutsaers, C. M. J.; Hart, C. M.; Matters, M.; de Leeuw, D. M. *Appl. Phys. Lett.* **1998**, *73*, 108.
(7) Bao, Z. N.; Rogers, J. A.; Katz, H. E. *J. Mater. Chem.* **1999**, *9*, 1895.
(8) Garnier, F.; Hajlaoui, R.; Yassar, A.; Srivastava, P. *Science* **1994**, *265*, 1684.
(9) Schön, J. H.; Berg, S.; Kloc, C.; Batlogg, B. *Science* **2000**, *287*, 1022.
(10) Lin, Y. Y.; Gundlach, D. J.; Nelson, S. F.; Jackson, T. N. *IEEE Trans. Electron Devices* **1997**, *44*, 1325.
(11) Kagan, C. R.; Mitzi, D. B.; Dimitrakopoulos, C. D. *Science* **1999**, *286*, 945.
(12) Sirringhaus, H.; Tessler, N.; Friend, R. H. *Science* **1998**, *280*, 1741.
(13) Lin, Y. Y.; Gundlach, D. J.; Nelson, S. F.; Jackson, T. N. *IEEE Electron Device Lett.* **1997**, *18*, 606.
(14) Schön, J. H.; Kloc, C.; Batlogg, B. *Phys. Rev. Lett.* **2001**, *86*, 3843.
(15) Chung, T. C.; Kaufman, J. H.; Heeger, A. J.; Wudl, F. *Phys. Rev. B* **1984**, *30*, 702.
(16) Brédas, J. L.; Themans, B.; Andre, J. M.; Chance, R. R.; Silbey, R. *Synth. Met.* **1984**, *9*, 265.
(17) Hill, M. G.; Mann, K. R.; Miller, L. L.; Penneau, J. F. *J. Am. Chem. Soc.* **1992**, *114*, 2728.
(18) Katz, H. E.; Bao, Z. N.; Gilat, S. L. *Accounts Chem. Res.* **2001**, *34*, 359.
(19) Campbell, R. B.; Trotter, J.; Robertson, J. M. *Acta Crystallogr.* **1961**, *14*, 705.
(20) Horowitz, G.; Bachet, B.; Yassar, A.; Lang, P.; Demanze, F.; Fave, J. L.; Garnier, F. *Chem. Mater.* **1995**, *7*, 1337.
(21) Siegrist, T.; Fleming, R. M.; Haddon, R. C.; Laudise, R. A.; Lovinger, A. J.; Katz, H. E.; Bridenbaugh, P.; Davis, D. D. *J. Mater. Res.* **1995**, *10*, 2170.

10.1021/cm020774+ CCC: $25.00
Published on Web 12/17/2002

explore new structures for high mobility, especially, the π-stacking structure.

Instead of aligning in the face-to-edge manner of the herringbone pattern, π-stacked molecules are situated in a face-to-face arrangement.[22] Clearly, such a packing configuration leads to stronger $\pi-\pi$ interactions between neighboring molecules. The larger $\pi-\pi$ interactions facilitate charge transfer between adjacent molecules by either of two mechanisms. At low temperatures, charge transport in crystalline materials appears to be coherent, i.e., band theory seems to be appropriate. At higher temperatures, phonon scattering leads to incoherent (hopping) transport.[1,14,23] Large $\pi-\pi$ interactions increase the carrier bandwidth (and, hence, the mobility) at low temperatures, and decrease hopping barriers at higher temperatures. Calculations show that the bandwidth for π-stacking structures could reach 0.2−0.4 eV, compared to the bandwidth of pentacene that is estimated to be 0.2 eV.[23−25] These values are still an order of magnitude smaller than those for inorganic semiconductors, e.g., Si, that have chemical bonds (1−3 eV) between neighboring atoms.

In this contribution, we develop several new materials for application in OTFTs. The materials are co-oligomers based on 4,4′-dialkyl-2,2′-bithiazole and 3,4-ethylenedioxythiophene (EDOT) in a donor−acceptor type molecule. Alkyl bithiazole oligomers crystallize with a "staircase" π-stack motif and may be reversibly n-doped,[26−29] whereas EDOT is a popular p-type material with low oxidation potential.[30,31] When the two moieties are connected in a donor−acceptor system, the resultant materials will be both p- and n-dopable, and may adopt the π-stacked structures characteristic of the bithiazoles. Thus, we synthesized several co-oligomers: the acceptor−donor−acceptor type, AT_2A (A = 4,4′-dialkyl-2,2′-bithiazole, T_2 = EDOT dimer). Specific alkylbithiazoles will be denoted by E = diethylbithiazole, B = dibutylbithiazole, and H = dihexylbithiazole. Also synthesized were donor−acceptor−donor type oligomers, TBT (T = EDOT, B = dibutylbithiazole) and T_2BT_2 (T_2 = EDOT dimer, B = dibutylbithiazole). Stille coupling reactions have been used successfully to prepare these compounds.[32] The full characterization of these materials has confirmed that the BT_2B oligomer is potentially a good candidate for high mobility organic semiconductors in OTFTs.

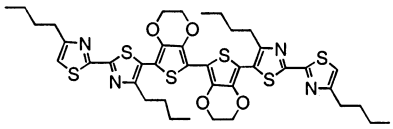

BT_2B

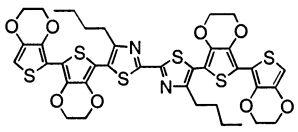

T_2BT_2

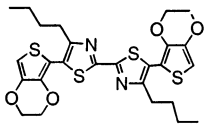

TBT

Experimental Section

Materials. All manipulations and preparations were performed under a nitrogen atmosphere using standard Schlenk line techniques unless otherwise stated. Reagents were purchased and used as received unless otherwise stated. Freshly opened, reagent grade solvents were dried by sequentially passing them through columns of molecular sieve (4A) and Cu/Al_2O_3 under a dry N_2 atmosphere. Synthesis of EDOT dimer $(EDOT)_2$,[31] 4,4′-dialkyl-2,2′bithiazoles, 5,5′-dibromo-4,4′-dialkyl-2,2′-bithiazole, and 5-trimethylstannyl-4,4′-dialkyl-2,2′-bithiazole were performed according to the literature procedures.[28] Synthesis of ET_2E and HT_2H are similar to that of BT_2B and are described in the Supporting Information.

^{1}H NMR spectra were collected on a Varian 300 or Varian 400 spectrometer and referenced to the residual solvent proton resonance. UV−vis spectra were collected on a Shimadzu 3101PC with baseline correction. Emission spectra were collected on a Shimadzu 4121 interfaced with a Gateway computer. Cyclic voltammetry (CV) was performed with a Princeton Applied Research Potentiostat model 263A interfaced to a PC computer. The solvent was dry CH_3CN or THF, and the supporting electrolyte was tetrabutylammonium hexafluorophosphate ($TBAPF_6$) (0.10 M). The reported potentials are vs the ferrocene/ferrocenium (Fc/Fc^+) couple, obtained by adding a crystal of ferrocene to the solution. Mass spectra were collected on a VG 70-250-s high-resolution spectrometer. Elemental analyses were performed by the University of Michigan Microanalysis Laboratory.

5,5′-Dibromo-2,2′-Bis(3,4-ethylenedioxythiophene) (Br−$(EDOT)_2$−Br). A 10-mL Schlenk flask equipped with a stirring bar was charged with $(EDOT)_2$ (500 mg, 1.77 mmol) in dry CH_2Cl_2 (60 mL). N-bromosuccinimide (NBS) (660 mg, 3.71 mmol) was added, and the reaction was allowed to stir at 0 °C for 2 h. The slightly blue mixture was dissolved in 500 mL of CH_2Cl_2 and washed by $NH_3{\cdot}H_2O$ (10%, 150 mL), H_2O (3 × 50 mL), and brine (2 × 50 mL), and dried over $MgSO_4$. The CH_2Cl_2 was evaporated (Rotovap) to give a yellowish solid that was stored in a drybox. Yield = 660 mg (85%). ^{1}H NMR ($CDCl_3$): δ 4.31 (8H,s).

5,5′-Bis(4,4′-dibutyl-2,2′-bithiazol-5-yl)−(3,4,3′,4′-bis-(ethylenedioxy)-2,2′-dithienyl) (BT_2B). (Dibutylbithiazole)-$SnMe_3$ (295 mg, 0.666 mmol) in dry toluene (60 mL) was added via cannula to a 100-mL Schlenk flask containing Br−$(EDOT)_2$−Br (130 mg, 0.30 mmol) and $Pd(PPh_3)_2Cl_2$ (21 mg, 0.03 mmol). The mixture was heated for 20 h during which time it turned dark red. After the mixture was cooled and filtered through Celite diatomaceous earth, the solvent was removed. The dark red solid was redissolved in CH_2Cl_2 and washed with HCl (5 wt %, 50 mL), H_2O (3 × 50 mL), NH_4Cl (saturated, 2 × 50 mL), and brine (2 × 50 mL), and dried over $MgSO_4$. The solvent was evaporated to give a red solid. Further purification involved a Soxhlet extraction with methanol to

(22) Hunter, C. A.; Sanders, J. K. M. *J. Am. Chem. Soc.* **1990**, *112*, 5525.
(23) Pope, M.; Swenberg, C. E. *Electronic Processes in Organic Crystals and Polymers*, 2nd ed.; Oxford University Press: New York, 1999.
(24) Silinsh, E. A.; Cápek, V. *Organic Molecular Crystals: Interaction, Localization and Transport Phenomena*; American Institute of Physics: Woodbury, NY, 1994.
(25) Brédas, J. L.; Beljonne, D.; Cornil, J.; Calbert, J. P.; Shuai, Z.; Silbey, R. *Synth. Met.* **2001**, *125*, 107.
(26) Koren, A. B.; Curtis, M. D.; Kampf, J. W. *Chem. Mater.* **2000**, *12*, 1519.
(27) Curtis, M. D.; Cheng, H. T.; Nanos, J. I.; Nazri, G. A. *Macromolecules* **1998**, *31*, 205.
(28) Nanos, J. I.; Kampf, J. W.; Curtis, M. D. *Chem. Mater.* **1995**, *7*, 2232.
(29) Yamamoto, T.; Suganuma, H.; Maruyama, T.; Inoue, T.; Muramatsu, Y.; Arai, M.; Komarudin, D.; Ooba, N.; Tomaru, S.; Sasaki, S.; Kubota, K. *Chem. Mater.* **1997**, *9*, 1217.
(30) Groenendaal, B. L.; Jonas, F.; Freitag, D.; Pielartzik, H.; Reynolds, J. R. *Adv. Mater.* **2000**, *12*, 481.
(31) Sotzing, G. A.; Reynolds, J. R.; Steel, P. J. *Adv. Mater.* **1997**, *9*, 795.
(32) Stille, J. K. *Angew. Chem. Int. Ed. Engl.* **1986**, *25*, 508.

remove most of the starting materials, followed by flash chromatography over silica gel with CH_2Cl_2 eluent to remove side-products. Bright red, single crystals were grown by slowly evaporating the solvent. Yield = 180 mg (71%). ^{1}H NMR ($CDCl_3$): δ 0.915 (6H, t, J = 7.2 Hz, $-CH_3$, outside), δ 0.95 (6H, t, J = 7.2 Hz, $-CH_3$, inner), δ 1.37 (4H, m, J = 7.6 Hz, $-CH_2-$, outside), δ 1.44 (4H, m, $-CH_2-$, inner), δ 1.69 (4H, m, $-CH_2-$, outside), δ 1.75 (4H, m, $-CH_2-$, inner), δ 2.78 (4H, t, J = 8 Hz, $-CH_2-$, outside), δ 2.98 (4H, m, J = 7.6 Hz, $-CH_2-$, inner), δ 4.36 (8H, t, J = 2 Hz, $-CH_2CH_2-$, EDOT ring), δ 6.90 (2H, s, 5-position ring proton). MS (EI): M^+ = 838.3. Elemental Analysis: calcd C, 57.3%; H, 5.53%; N, 6.67%; found C, 57.1%; H, 5.63%; N, 6.61%.

2-(Trimethylstannyl)-3,4-(ethylenedioxy)thiophene. In a 100-mL Schlenk flask, was placed a 2.0 g (14.1 mmol) sample of 3,4-(ethylenedioxy)thiophene in 50 mL of dry THF. A solution (6.2 mL, 15.5 mmol) of 2.5 M *n*-butyllithium was added dropwise into the EDOT solution at −78 °C under nitrogen. After the solution was stirred for 1 h, it was allowed to warm to −40 °C, and 3.37 g (16.9 mmol) of trimethylstannyl chloride was added to the solution. The solvent was removed via Rotovap after the solution was stirred overnight. After the solvent was evaporated, the residue was dissolved in hexane and washed with H_2O (3 × 30 mL), then brine (2 × 30 mL), and dried over $MgSO_4$. The product was a white solid after the solvent was evaporated in a vacuum. Yield = 3.60 g (84%). ^{1}H NMR ($CDCl_3$): δ 0.31 (9H, s, $-SnMe_3$), δ 4.14 (4H, t, J = 8.0 Hz, $-CH_2-$ on EDOT ring), δ 6.55 (1H, s, 5-position ring proton). Elemental analysis: calcd C, 35.5%; H, 4.63%; found C, 34.7%; H, 4.54%.

5,5′-Bis(3,4-ethylenedioxythien-2-yl)-4,4′-dibutyl-2,2′-bithiazole (TBT). In a 100-mL Schlenk flask equipped with a reflux condenser and nitrogen outlet, was placed (EDOT)-$SnMe_3$ (146 mg, 0.479 mmol), Br−(Dibutylbithiazole)−Br (100 mg, 0.228 mmol), and $Pd(PPh_3)_2Cl_2$ (16 mg, 0.02 mmol), and dry toluene (60 mL). The mixture was heated to reflux for 16 h, after which time the solution showed a green fluorescence. After cooling to room temperature, the toluene solution was washed with HCl solution (5%, 50 mL), H_2O (3 × 30 mL), saturated NH_4Cl solution (2 × 30 mL), then brine (2 × 30 mL), and dried over $MgSO_4$. The solvent was removed by Rotovap to give an orange solid. Then, the raw product in CH_2Cl_2 was run through a chromatography column filled with silica gel for further purification. Yield = 109 mg (85%). ^{1}H NMR ($CDCl_3$): δ 0.944 (6H, t, J = 7.2 Hz, $-CH_3$), δ 1.44 (4H, m, J = 7.2 Hz, $-CH_2-$), δ 1.75 (4H, m, J = 7.2 Hz, $-CH_2-$), δ 2.95 (4H, t, $-CH_2-$), δ 4.26 (4H, m, J = 2.7 Hz, $-CH_2$ on EDOT ring), δ 4.32 (4H, m, J = 2.7 Hz, $-CH_2$ on EDOT ring), δ 6.41 (2H, s, EDOT ring proton at 5-position). Elemental analysis: calcd C, 55.7%; H, 5.03%; N, 4.99%; found C, 55.8%; H, 5.09%; N, 4.85%.

5,5′-Bis(5-bromo-3,4-ethylenedioxythien-2-yl)-4,4′-dibutyl-2,2′-bithiazole (Br−TBT−Br). A 100-mL Schlenk flask equipped with a stirring bar was charged with TBT (100 mg, 0.178 mmol) in CH_2Cl_2 (60 mL). N-bromosuccinimide (NBS) (67 mg, 0.376 mmol) was added, and the reaction was allowed to stir at 0 °C and under exclusion of light for 2 h. After the solvent was evaporated, the raw product was washed with acetone to remove the extra starting materials to give an orange solid. Yield = 121 mg (95%). ^{1}H NMR ($CDCl_3$): δ 0.94 (6H, t, J = 7.2 Hz, $-CH_3$), δ 1.25 (4H, m, J = 7.2 Hz, $-CH_2-$), δ 1.75 (4H, m, J = 7.2 Hz, $-CH_2-$), δ 2.95 (4H, t, $-CH_2-$), δ 4.32 (8H, m, $-CH_2$, EDOT ring). Elemental analysis: calcd C, 43.5%; H, 3.65%; N, 3.90%; found C, 45.3%; H, 4.16%; N, 4.04%.

5,5′-Bis(3,4,3′,4′-bis(ethylenedioxy)-2,2′-dithien-5-yl)-4,4′-dibutyl-2,2′-bithiazole (T_2BT_2). In a 100-mL Schlenk flask equipped with a reflux condenser and nitrogen outlet, was placed (EDOT)-$SnMe_3$ (94 mg, 0.308 mmol), Br−TBT−Br (100 mg, 0.139 mmol), $Pd(PPh_3)_2Cl_2$ (20 mg, 0.03 mmol), and dry toluene (60 mL). The mixture was heated to reflux for 12 h. After cooling to room temperature, the solution was washed with HCl solution (5%, 50 mL), H_2O (3 × 30 mL), saturated NH_4Cl solution (2 × 30 mL), then brine (2 × 30 mL), and dried over $MgSO_4$. The solvent was removed by Rotovap to give an orange solid. Then, the raw product in CH_2Cl_2 was run through a chromatography column filled with silica gel for further purification. Yield = 109 mg (93%). ^{1}H NMR ($CDCl_3$): δ 0.976 (6H, t, J = 7.2 Hz, $-CH_3$), δ 1.45 (4H, m, J = 7.2 Hz, $-CH_2-$), δ 1.79 (4H, m, J = 7.2 Hz, $-CH_2-$), δ 3.00 (4H, t, J = 7.8 Hz, $-CH_2-$), δ 4.25−4.39 (16H, m, $-CH_2$, EDOT ring), δ 6.32 (2H, s, EDOT ring proton at 2-position). Elemental analysis: calcd C, 54.3%; H, 4.31%; N, 3.33%; found C, 53.2%; H, 4.65%; Nn 3.18%.

Scheme 1. Synthesis of AT_2A Oligomers: (a) BuLi/−78 °C/THF, $CuCl_2$; (b) NBS/CH_2Cl_2/0 °C; (c) BuLi/−78 °C/THF, $SnMe_3Cl$; (d) Stille Coupling, $Pd(PPh_3)_2Cl_2$/Toluene/20 h

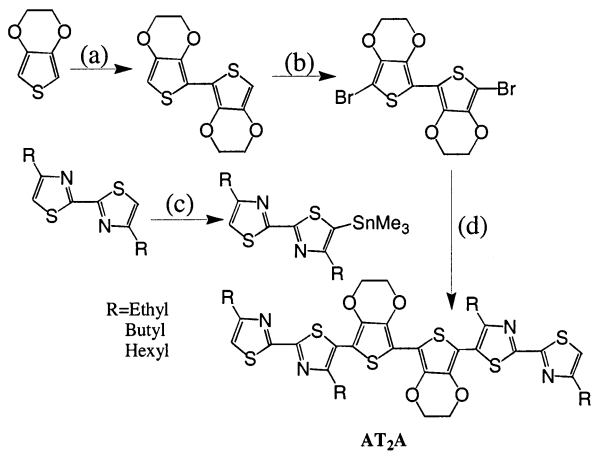

AT_2A

Results and Discussion

Preparation. All these co-oligomers of alky-bithiazoles and EDOT were prepared using Stille coupling reactions. AT_2A oligomers were synthesized as shown in Scheme 1. The coupling between the diallkylbithiazole−$SnMe_3$ and Br−$(EDOT)_2$−Br required a high reaction temperature because the bithiazole-tin reagents are poor nucleophiles. Thus, toluene was chosen as the solvent in most of our coupling reactions, as reactions in THF gave very low yields (∼20%). The yields of the coupling reactions are reasonably high, except for ET_2E. It is necessary to have pure reactants to achieve high yields. Using less than 1 equiv of BuLi per bithiazole in the lithiation reaction decreased the amount of ditin bithiazole formed by unintentional dilithiation. Furthermore, because of the low oxidation potential of $(EDOT)_2$, Br−$(EDOT)_2$−Br must be prepared at 0 °C with exclusion of light to prevent over-oxidation or polymerization by NBS. Reducing the crude product and removal of the NBS with $NH_3{\cdot}H_2O$ is recommended. However, the AT_2A oligomers are reasonably stable due to the electron-withdrawing bithiazole groups attached to the $(EDOT)_2$ core that block the reactive 5,5′-positions of $EDOT_2$. The products with butyl and hexyl side-chains are very soluble in many common solvents, e.g., toluene, and $CHCl_3$, making them suitable for liquid-phase spin-coating.

The syntheses of TBT and T_2BT_2 are shown in Scheme 2. The Stille coupling reactions in this series gave better yields than those obtained for BT_2B because (EDOT)−$SnMe_3$ is a better nucleophile than (dibutylbithiazole)−$SnMe_3$. Adding a slight excess of (EDOT)−$SnMe_3$ reduced the amount of monosubstituted product that formed during the coupling reaction.

Table 1. Characterization of Five Co-Oligomers on the Basis of WAXD Pattern, UV Absorption, Emission Maximum Wavelength, and Optical Band Gap

		UV absorption eV (nm)		emission eV (nm)	optical band gap (eV)	
name	WAXD peaks (2θ) and d-spacing	soln	film	soln	soln	film
ET_2E	4.4°(20.0 Å), 8.1°(10.9 Å) 8.5°(10.4 Å), 9.7°(9.1 Å) 12.7°(7.0 Å), 17.1°(5.2 Å) 21.2°(4.2 Å), 25.1°(3.5 Å)	2.69 (461)	2.69 (461) 2.48 (500) 2.25 (551)	2.23 (556)	2.28	2.00
BT_2B	6.3°(14.0 Å), 10.9°(8.1 Å) 18.9°(4.7 Å), 22.5°(3.9 Å) 25.1°(3.5 Å)	2.66 (466)	2.61 (475) 2.46 (504) 2.30 (539)	2.12 (585)	2.30	2.08
HT_2H	5.0°(17.7 Å), 9.8°(9.0 Å) 17.5°(4.1 Å), 21.9°(4.1 Å) 25.2°(3.5 Å)	2.66 (466)	2.66 (466) 2.50 (496) 2.30 (539)	2.12 (585)	2.30	2.10
TBT		3.02 (411)	3.03 (409) 2.86 (434) 2.63 (471)	2.57 (482) 2.45 (506)	2.60	2.46
T_2BT_2		2.66 (466)	2.65 (468), 2.50 (496), 2.30 (539)	2.24 (554) 2.12 (585)	2.24	2.10

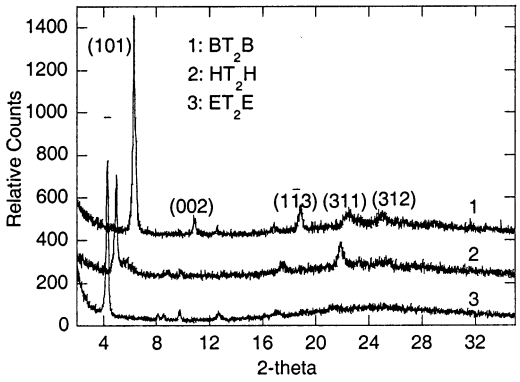

Figure 1. WAXD patterns of solution-cast films of ET_2E, BT_2B, and HT_2H.

The only successful route to T_2BT_2 was the coupling between (EDOT)−$SnMe_3$ and Br−TBT−Br. Attempts at coupling $(EDOT)_2$−$SnMe_3$ and Br−(dibutylbithiazole)−Br failed because of the low stability of $(EDOT)_2$−$SnMe_3$. Fortunately, Br−TBT−Br was easy to prepare by bromination of TBT by NBS. Because Br−TBT−Br was only partially soluble in toluene, the coupling reaction had to be done at reflux temperature. Both compounds, TBT and T_2BT_2, are quite soluble and stable enough for further characterization.

X-ray Diffraction. Since the crystal structure of BT_2B has been solved recently,[33] the film orientation could be studied based on the wide-angle X-ray diffraction (WAXD) patterns. Figure 1 shows an overlay of the WAXD patterns of AT_2A solution-cast films. The 2θ and d values are collected in Table 1. BT_2B shows XRD peaks at $2\theta = 6.3°$, 10.9°, 18.9°, 22.5°, and 25.1°, corresponding to 14.0, 8.1, 4.7, 3.9, and 3.5 Å, respectively. These peaks could be assigned to the $(\bar{1}01)$, (002), $(\bar{1}13)$, (311), and (312) reflections by comparison to the X-ray powder pattern simulated from the single-crystal structure (Supporting Information). The d spacing corresponding to the peak at $2\theta = 25.1°$ is similar to the π-stacking distance measured from the single-crystal structure.

There is also a strong diffraction peak at $2\theta = 5.0°$ from HT_2H films, corresponding to the lamellar structure with a d spacing of 17.7 Å. The longer hexyl sidechain is expected to expand the lamellar distance. Other peaks of HT_2H are located at 2θ of 9.8°, 17.5°, 21.9°, and 25.2°, and these match the d spacings of 9.0, 5.1, 4.1, and 3.5 Å in the butyl derivative. It thus appears that the butyl and hexyl derivatives are isomorphous.

The structure of ET_2E appears to be similar, but not isomorphous, to those of the butyl and hexyl compounds. A strong peak at $2\theta = 4.4°$ (20 Å) is observed, but the 20 Å distance is not compatible with a simple lamellar spacing between ethyl-substituted oligomers. Other peaks are located at 2θ of 8.1°, 8.5°, 9.7°, 12.7°, 17.1°, 21.2°, and 25.1°, corresponding to 10.9, 10.4, 9.1 7.0, 5.2, 4.2, and 3.5 Å. However, the peak corresponding to the π-stacking distance (3.5 Å) still can be observed, implying that ET_2E also forms π-stacks.

Scheme 2. Synthesis of TBT and T_2BT_2 Oligomers: (a) $Br_2/CHCl_3$/Reflux/2 h; (b) BuLi/−78 °C/THF, $SnMe_3Cl$; (c) Stille Coupling, $Pd(PPh_3)_2Cl_2$/Toluene/16 h; (d) NBS/CH_2Cl_2/0 °C/Dark; (e) Stille Coupling, $Pd(PPh_3)_2Cl_2$/Toluene/16 h

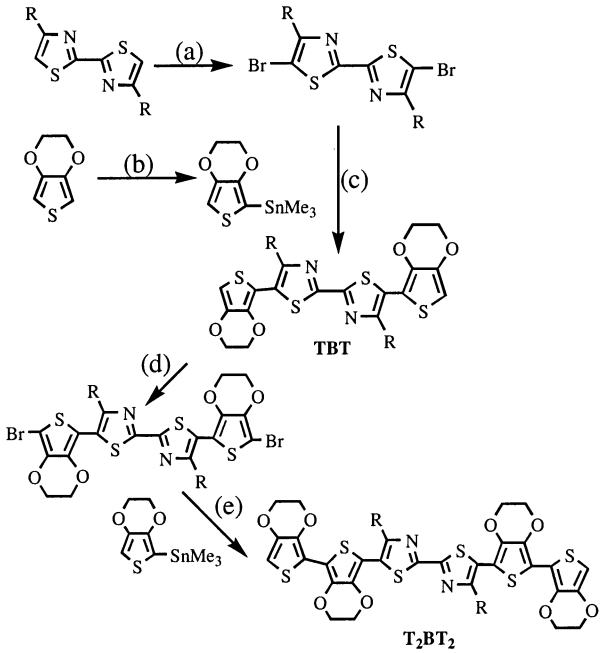

UV−Vis Spectroscopy. Figures 2 and 3 display the UV−vis spectra of solutions and solid films of these

(33) Cao, J.; Kampf, J. W.; Curtis, M. D. **2002**, manuscript in preparation.

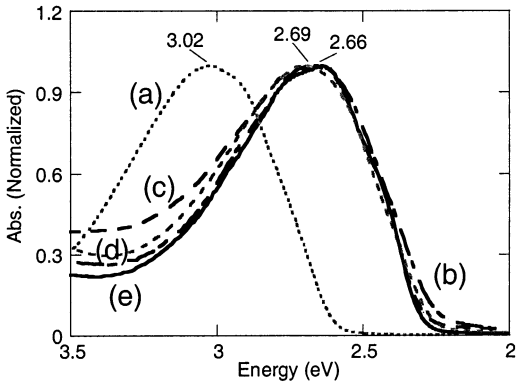

Figure 2. UV−vis absorption spectra of AT_2A, TBT, and T_2BT_2 oligomers in solution: (a) TBT, (b) T_2BT_2, (c) ET_2E, (d) BT_2B, and (e) HT_2H.

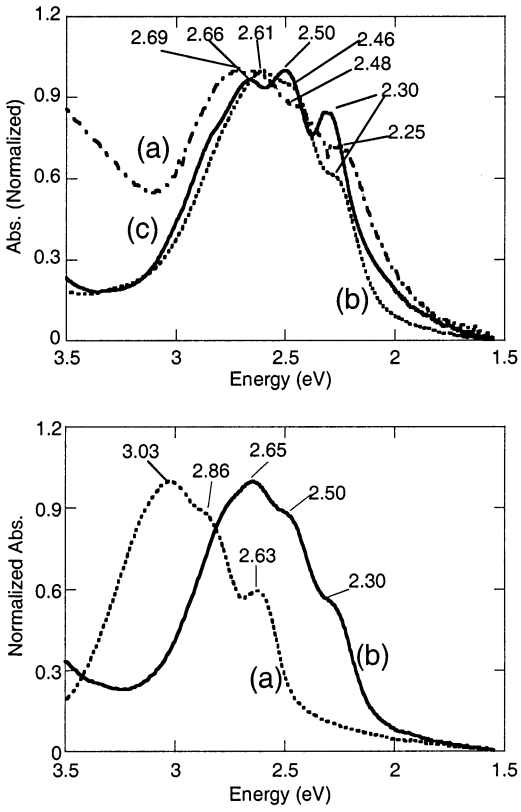

Figure 3. UV−vis absorption spectra of the oligomer films. Top: (a) ET_2E, (b) BT_2B, and (c) HT_2H. Bottom: (a) TBT and (b) T_2BT_2.

oligomers, and the results are summarized in Table 1. As expected, the length of alkyl side-chains slightly influenced the absorption spectra of AT_2A compounds in both solution and the solid state. For example, ET_2E in solution gave an absorption maximum at 2.69 eV (461 nm), which is 0.03 eV blue-shifted compared to BT_2B and HT_2H, both of which absorb at 2.66 eV (466 nm). Interestingly, if we compare two oligomers having the identical side-chains, T_2BT_2 and BT_2B, there is no difference in solution UV absorption maxima as both occur at 2.66 eV. The donor−acceptor sequence seems to have little influence on the solution absorption, as long as the number of the conjugated rings is the same. Compared to the corresponding donor or acceptor oligomers, the donor−acceptor systems have clearly lowered the energy of the optical transition. For instance, butyl bithiazole trimer (B_3), a typical acceptor oligomer,

Table 2. Estimates of Davydov Splitting (W_D) and Interchain Transfer Integral (β) from the Solid-State Absorption Spectra and Solution Emission Spectra[a]

name	W_D (eV)	ΔE_{abs} (eV)	ΔE_{em} (eV)	β (meV)
ET_2E	0.21	1.34	0.75	95
BT_2B	0.15	1.08	0.58	88
HT_2H	0.16	1.10	0.60	85
TBT	0.17	1.06	0.75	35
T_2BT_2	0.15	1.10	0.73	55

[a] ΔE_{abs} and ΔE_{em} represent the measured widths of the absorption and emission peaks, respectively.

shows an absorption maximum at 3.27 eV (379 nm), compared to 2.66 eV for BT_2B. Because of the fewer conjugated rings in its backbone, a significant blue shift was observed in the absorption maximum of TBT at 3.02 eV (410 nm) compared to 2.66 eV (466 nm) for BT_2B.

The UV spectra in solid films are dependent on the solid-state morphology, in particular, whether the molecules are π-stacked.[34] In the series of AT_2A, the absorption peaks are all shifted to lower energies with respect to the solution because molecular chains adopt a more planar conformation in the solid state. ET_2E, BT_2B, and HT_2H share a 3-peak pattern with maxima located at 2.69, 2.48, and 2.25 eV (461, 500, and 551 nm, respectively) for ET_2E, 2.61, 2.48, and 2.30 eV (475, 500, and 539 nm, respectively) for BT_2B, and 2.66, 2.50, and 2.30 eV for HT_2H (466, 496, and 539 nm, respectively). The compounds, TBT and T_2BT_2, also have a 3-peak pattern similar to that of BT_2B. The peak maxima are situated at 3.03, 2.86, and 2.63 eV (409, 434, and 471 nm, respectively) for TBT and 2.65, 2.50, and 2.30 eV (468, 496, and 539 nm, respectively) for T_2BT_2. The origin of the multi-peaks has been explained by exciton band theory.[26,34−39] If there is more than one molecule per unit cell, the absorption peaks are split into one allowed transition for each translationally inequivalent molecule (Davydov splitting). Phonon coupling may relax the $\Delta k = 0$ selection rule (k = wavevector for the exciton band) with the result that the absorption peak samples the density of states in the exciton band. This, combined with the Davydov splitting (W_D), results in a 3-band pattern if there are two molecules per unit cell.[39]

The Davydov splitting can be estimated from the film absorption spectra, i.e. the separation of the peaks from the two high-energy exciton branches.[26] For example, in the case of BT_2B, the Davydov splitting is about 0.15 eV ($W_D = 2.61 - 2.46 = 0.15$ eV). The values of the five co-oligomers are in the range of 0.15−0.21 eV, as collected in Table 2, which are larger than those normally found in organic crystals such as anthracene. Our recent study shows that the interchain transfer integral, β, can also be estimated from the solid-state

(34) Politis, J. K.; Nemes, J. C.; Curtis, M. D. *J. Am. Chem. Soc.* **2001**, *123*, 2537.
(35) Beljonne, D.; Langeveld-Voss, B. M. W.; Shuai, Z.; Janssen, R. A. J.; Meskers, S. C. J.; Meijer, E. W.; Bredas, J. L. *Synth. Met.* **1999**, *102*, 912.
(36) Bosisio, R.; Botta, C.; Colombo, A.; Destri, S.; Porzio, W.; Grilli, E.; Tubino, R.; Bongiovanni, G.; Mura, A.; DiSilvestro, G. *Synth. Met.* **1997**, *87*, 23.
(37) DiCesare, N.; Belletete, M.; Marrano, C.; Leclerc, M.; Durocher, G. *J. Phys. Chem. A* **1999**, *103*, 795.
(38) Spano, F. C.; Siddiqui, S. *Chem. Phys. Lett.* **1999**, *314*, 481.
(39) Koren, A. B.; Kampf, J.; Curtis, M. D. **2002**, submitted for publication.

Table 3. Cyclic Voltammetry of Five Oligomers as Measured in THF/TBAPF$_6$ Solution; Potentials are Referenced to Fc/Fc$^+$ Couple

	oxidation (V vs Fc/Fc$^+$)			reduction (V vs Fc/Fc$^+$)			band gap (eV)
name	$E_{ox}{}^p$	$E^{1/2}{}_{ox}$	ΔE_p	$E_{red}{}^p$	$E^{1/2}{}_{red}$	ΔE_p	$E_g{}^{CV}$
ET_2E	0.282			−2.45	−2.37	0.16	2.7
	0.403						
BT_2B	0.302	0.262	0.080	−2.38	−2.31	0.15	2.6
	0.761	0.724	0.075				
HT_2H	0.316	0.281	0.071	−2.37	−2.32	0.11	2.6
	0.656	0.593	0.13				
TBT	0.637			−2.42	−2.31	0.22	2.9
T_2BT_2	0.130			−2.35	−2.26	0.18	2.4
	0.220						

absorption and emission spectra which are discussed elsewhere.[39] The value of 4β can be obtained from eq 1

$$4\beta = W_{abs} - \Delta E_{em} \quad (1)$$

where W_{abs} and ΔE_{em} correspond to the width of the solid-state absorption and emission spectra, respectively. The effect of the Davydov splitting has been subtracted from the measured width of absorption spectra: $W_{abs} = \Delta E_{abs} - W_D$. The values of β, as listed in Table 2, imply that AT_2A oligomers ($\beta \approx 90$ meV) may have stronger interchain interactions than TBT or T_2BT_2 ($\beta = 35$ or 55 meV) and, in the donor−acceptor−donor series, β increases as the chain length increases. We have used the ZINDO method to estimate the interchain interactions of π-stacks, and the magnitudes of the calculated transfer integrals are comparable to those found experimantally.[40] It is interesting to note that the fine structures seen in ET_2E, BT_2B, and HT_2H film absorption spectra imply that the molecules are π-stacked, and that there are two molecules per unit cell—features that are confirmed by the solved crystal structure of BT_2B.[33] Therefore, we may also predict that the solid-state structures of TBT and T_2BT_2 feature molecules that are π-stacked with two inequivalent molecules per unit cell.

Emission spectra of solutions of the co-oligomers AT_2A are shown in Figure 4, and the results are also summarized in Table 1. ET_2E has an emission maximum at 2.23 eV (556 nm). The maxima for BT_2B and HT_2H are nearly identical at 2.12 eV (585 nm), and the spectrum of BT_2B also displays a small shoulder near 2.20 eV (564 nm). As expected, the high-energy edges of the emission from all three co-oligomers overlap the low-energy feet of their corresponding absorption peaks (overlap of the 0−0 vibronic transitions). However, in the cases of TBT and T_2BT_2 oligomers, multiple peaks were detected in emission spectra. TBT has maxima at 2.57 and 2.45 eV (482 and 506 nm, respectively), whereas T_2BT_2 emits at somewhat lower energy values: 2.24 eV (554 nm) and 2.12 eV (585 nm). Compared to their absorption spectra, the high-energy edges of the emission also overlap the low-energy feet of their corresponding absorption peaks, but the Stokes shifts are larger than those of AT_2A compounds, implying a large degree of out-of-plane ring torsion in the ground state of TBT and T_2BT_2.

The band gaps of these co-oligomers were estimated by extrapolation of the low energy edge of the absorption spectra to the baseline and are also collected in Table 1. Both BT_2B and HT_2H have the same band-gaps (2.3 and 2.1 eV for the solution and solid state, respectively), whereas ET_2E gives a little smaller value (2.28 and 2.00 eV for the solution and solid-state, respectively). In the case of T_2BT_2, the values are very similar to BT_2B and HT_2H (2.24 and 2.10 eV for the solution and solid-state, respectively). As expected, the smallest oligomer, TBT, has the highest band gap (2.60 and 2.46 eV for the solution and solid-state, respectively) due to its shorter conjugation length.

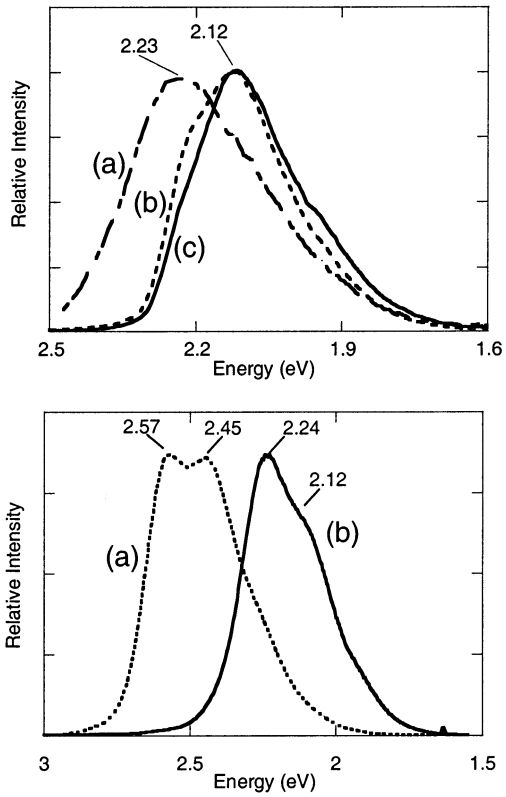

Figure 4. Emission spectra of the oligomers in dilute $CHCl_3$ solution. Top: (a) ET_2E, (b) BT_2B, and (c) HT_2H. Bottom: (a) TBT and (b) T_2BT_2.

Electrochemistry. Cyclic voltammetry (CV) measurements were carried out to determine the redox behavior of the oligomers, and the results are shown in Table 3. The oxidation and reduction waves of the AT_2A materials in 0.1 M THF/TBAPF$_6$ solutions are displayed in Figures 5 and 6. As expected, the acceptor−donor−acceptor type oligomers, AT_2A, can be both oxidized and reduced within the potential range of the solvent/electrolyte window. In solution, all three AT_2A oligomers have two oxidation waves. HT_2H has one reversible oxidation near $E^{1/2}{}_{ox} = 0.281$ V ($\Delta E_p = 71$ mV) and a

(40) Cao, J.; Curtis, M. D. **2002**, manuscript in preparation.

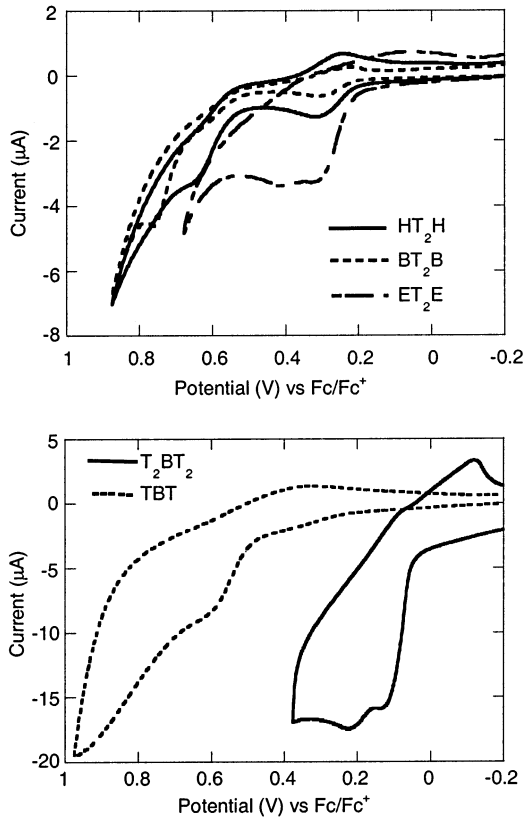

Figure 5. Oxidation cyclic voltammetry waves of the oligomers at 50 mV/s scan rate in THF/$TBAPF_6$ solution. Top: three AT_2A oligomers. Bottom: TBT and T_2BT_2.

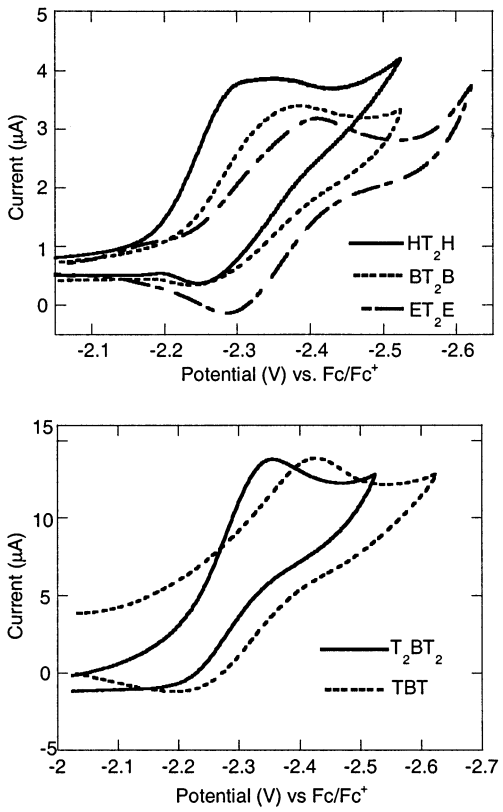

Figure 6. Reduction cyclic voltammetry waves of the oligomers at 50 mV/s scan rate in THF/$TBAPF_6$ solution. Top: three AT_2A oligomers. Bottom: TBT and T_2BT_2.

quasi-reversible oxidation at $E^{1/2}_{ox} = 0.593$ V (ΔE_p = 130 mV) vs the ferrocene/ferrocenium couple (Fc^+/Fc, 0.1 M Bu_4NPF_6 ($TBAPF_6$) in THF as the supporting electrolyte). Similarly, BT_2B also shows two quasi-reversible oxidations around $E^{1/2}_{ox} = 0.262$ V (ΔE_p = 80 mV) and $E^{1/2}_{ox} = 0.724$ V ($\Delta E^p_{ox} = 75$ mV). These two quasi-reversible couples correspond to 1e-oxidations to form cation radical and di-cations, respectively. The potential could be cycled repeatedly with no change in the CV curves. However, the oxidation behavior of ET_2E is quite different from that of BT_2B or HT_2H. ET_2E has two resolvable oxidation waves at $E^p_{ox} = 0.282$ and 0.403 V and one returning reduction wave at 0.113 V. The oxidation waves of ET_2E drift to more positive values by almost 60 mV after being cycled for 10 times, instead of being invariant as in HT_2H and BT_2B. We ascribe these changes to the formation of a film of the oxidized material on the electrode surface. The longer alkyl side chains apparently inhibit film formation. Despite the variation in the oxidation behavior, the reduction cycles are very similar among the three compounds. HT_2H displays a quasi-reversible reduction near $E^{1/2}_{red} = -2.32$ V (ΔE^p_{red} = 110 mV). BT_2B shows an almost identical reduction potential at $E^{1/2}_{red} = -2.31$ V (ΔE^p_{red} = 150 mV), and ET_2E displays very little difference, with a reduction potential at $E^{1/2}_{red} = -2.37$ V (ΔE^p_{red} = 160 mV).

Compared with the acceptor−donor−acceptor type of structures, the donor−acceptor−donor compounds, TBT and T_2BT_2, show quite different oxidation behavior. Both compounds show electrochemical irreversibility during the oxidation cycle. TBT gave an oxidation at $E_{ox} = 0.637$ V and a returning reduction at $E_{red} = 0.347$ eV, whereas T_2BT_2 had two oxidations at 0.130 and 0.220 V with a returning E_{red} at −0.12 V. A more detailed study of the spectroelectrochemical and chemical oxidations of these compounds will be reported separately.[40] Both TBT and T_2BT_2 had similar quasi-reversible reduction potentials at $E^{1/2}_{red} = -2.31$ V ($\Delta E^p_{red} = 220$ mV) and $E^{1/2}_{red} = -2.26$ V ($\Delta E^p_{red} = 180$ mV), respectively. Regardless of the donor−acceptor sequence of these co-oligomers, EHMO calculations suggest that the positive charge is mostly located on the EDOT rings after oxidation of the co-oligomers, a result that is confirmed by ESR experiments.[40]

Scheme 3. Energy Diagram of the Co-oligomers, Based on Their Threshold Oxidation and Reduction Potentials and the Low-energy UV−Vis Absorption Thresholds

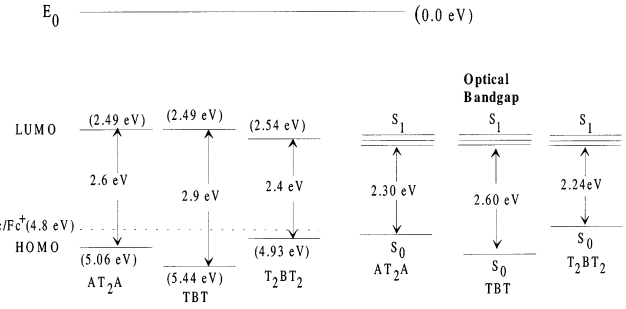

The band gaps determined from CV are similar to the optical band gaps obtained from extrapolation of the low-energy edge of the UV−vis absorption. An approximate energy diagram, illustrated in Scheme 3, is based on the CV and UV−vis data. The band gaps calculated from CV are 2.6, 3.0, and 2.4 eV, compared

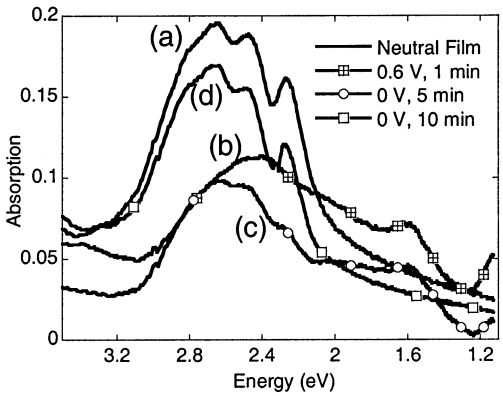

Figure 7. Spectroelectrochemical measurement of BT_2B films: (a) neutral film, (b) 0.60 V for 1 min, (c) 0.0 V for 5 min, and (d) 0.0 V for 10 min.

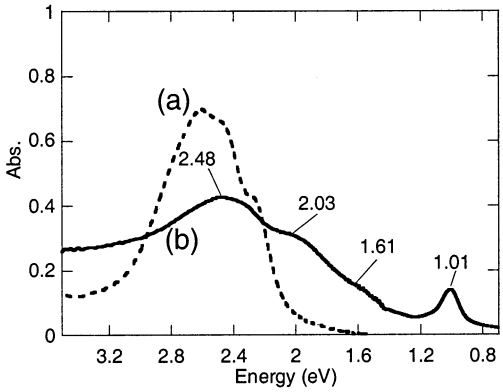

Figure 8. I_2 doping of BT_2B films made by vacuum deposition: (a) neutral film, (b) doped by I_2 vapor for 3 h.

with the corresponding optical band gaps: 2.3, 2.6, and 2.2 eV for AT_2A, TBT, and T_2BT_2, respectively.

A spectroelectrochemical study of the oligomer films was undertaken, and the results for BT_2B are shown in Figure 7. A film of BT_2B was dip-coated onto an ITO electrode and the measurements were conducted in a cell containing a 0.1 M $TBAPF_6$ solution in acetonitrile. The spectra of the films changed rapidly after voltage was applied. At 0.60 V, the intensities of the peaks of the neutral film decreased, while new peaks grew in at 2.4, 1.6, and 1.1 eV (517, 775, and 1127 nm, respectively). Upon resetting the voltage to 0.0 V, the film starts to de-dope as evidenced by the decrease in the intensities of the peaks assigned to the oxidized species and the concomitant growth of the peaks due to the neutral material. The fact that the fine structure, caused by the details of molecular packing, is regenerated also is strong evidence that the cycle of oxidation/reduction does not alter the solid-state packing. This means that the dopant ions (PF_6^-) most likely move into the channels that are parallel to the π-stacks. The de-doping process is relatively slow: it takes about 10 minutes after switching the voltage back to 0.0 V for the film to be fully reduced. After a doping/dedoping cycle, the intensity of the absorption peak is a little lower than that of the fresh sample, most likely because a small amount of oxidized film detaches from the ITO electrode in acetonitrile solution and is not reduced.

Solid-state films can also be doped by chemical means, e.g., I_2 vapor. Figure 8 displays the UV−NIR spectra of BT_2B film made by vapor deposition before and after I_2 doping. Compared to the spectroelectrochemical changes observed in Figure 7, the chemical doping causes a similar spectral change. The peaks of the neutral oligomer are replaced by peaks at 2.48 and 1.01 eV (500 and 1228 nm) along with broad shoulders at 2.03 and 1.61 eV (611 and 770 nm). The explanation of the spectral changes in the oxidized films in terms of configuration interaction of the excited states of the radical cations has recently been made.[25]

The conductivities of the I_2-doped BT_2B films (about 1 μm to 5 μm thick) were measured. The films were cast from $CHCl_3$ onto glass slides and doped by I_2 vapor for 3 h. The doped films gave conductivities of about 1×10^{-2} S/cm^{-1} as measured by the standard 4-point probe method. The conductivity is lower than that of EDOT polymer,[30] possibly due to the roughness of the solution cast films that introduces high grain-boundary resistance.

Conclusions

Alkyl-bithiaozle and $(EDOT)_2$ co-oligomers, AT_2A, have been synthesized by Stille coupling reactions. The addition of alkyl-bithiazole units induces the co-oligomers to form π-stacked crystal structures with short intermolecular contact distances (e.g., 3.5 Å measured for the BT_2B crystal) and good $\pi-\pi$ overlap. Analysis of the X-ray diffraction pattern of the films deposited on a hydrophilic substrate shows that the π-stacking axis is parallel to the substrate with the conjugated rings tilted with respect to the substrate. The incorporation of the EDOT dimer unit into the oligomers imparts a low oxidation potential. Because the bithiazole groups have a reasonably low reduction potential, the combination of low energy LUMO acceptor (bithiazole) with high energy HOMO donor (EDOT) leads to a lowered band gap. The electrochemical characterization demonstrates that either p-doping or n-doping is possible for these oligomers. BT_2B and HT_2H oligomers display quasi-reversible electrochemical behavior, whereas ET_2E, ATA, and T_2BT_2 oligomers show more complex behavior. All these features make these new materials promising for use in organic-based TFTs. The fabrication and characterization of OTFTs with BT_2B as the active semiconductors will be reported elsewhere.

Acknowledgment. This research was supported by the National Science Foundation (DMR-9986123).

Supporting Information Available: General experimental and synthetic procedures and crystallographic data tables of BT_2B. This material is available free of charge via the Internet at http://pubs.acs.org.

CM020774+